Published by Institute of Physics Publishing for SISSA/ISAS
Received: *March 5, 2004*
Revised: *April 29, 2004*
Accepted: *May 4, 2004*

Density matrix renormalization group in a two-dimensional $\lambda\phi^4$ hamiltonian lattice model

Takanori Sugihara

RIKEN BNL Research Center, Brookhaven National Laboratory
Upton, New York 11973, U.S.A.
E-mail: sugihara@bnl.gov

Abstract: Density matrix renormalization group (DMRG) is applied to a (1 + 1)-dimensional $\lambda\phi^4$ model. Spontaneous breakdown of discrete Z_2 symmetry is studied numerically using vacuum wavefunctions. We obtain the critical coupling $(\lambda/\mu^2)_c = 59.89 \pm 0.01$ and the critical exponent $\beta = 0.1264 \pm 0.0073$, which are consistent with the Monte Carlo and the exact results, respectively. The results are based on extrapolation to the continuum limit with lattice sizes $L = 250, 500$, and 1000. We show that the lattice size $L = 500$ is sufficiently close to the the limit $L \to \infty$.

Keywords: Renormalization Group, Field Theories in Lower Dimensions, Spontaneous Symmetry Breaking, Lattice Gauge Field Theories.

Contents

JHEP05(2004)007

1. Introduction

Hamiltonian diagonalization is a useful method for nonperturbative analysis of many-body quantum systems [1, 2]. If hamiltonian is diagonalized, the system can be analyzed nonperturbatively at the amplitude level using the obtained wave functions [3]–[7]. In addition, one can discuss associated symmetry based on operator algebra [8, 9]. However, in general quantum field theories, the method does not work without reducing degrees of freedom because the dimension of hamiltonian increases exponentially as the system size becomes large. There is a severe limitation on numerical diagonalization of hamiltonian. To apply the method to quantum field theories, we need to find a way to remove unimportant degrees of freedom and create a small number of optimum basis states. This is the concept of renormalization group.

Wilson's numerical renormalization group applied to the Kondo problem was a successful consideration along this line [10]. To analyze chain models other than Kondo hamiltonian, White proposed density matrix renormalization group (DMRG) as an extension of the Wilson's method [11, 12]. In DMRG, calculation accuracy of the target state can be controlled systematically using density matrices. White calculated energy spectra and wavefunctions of Heisenberg chains composed of more than 100 sites using a standard workstation. The DMRG analysis of a 100-site $S = 1/2$ chain corresponds to diagonalization of hamiltonian with $2^{100} \sim 10^{30}$ dimensions. DMRG has been applied to various one-dimensional models, such as Kondo, Hubbard, and t-J chain models, and achieved great success. A two-dimensional Hubbard model has also been studied with DMRG in both real- and momentum-space representation [13, 14]. DMRG works well on small two-dimensional lattices and new techniques have been proposed for larger lattices. DMRG has also been extended to finite-temperature chain models using the transfer-matrix technique based on the Suzuki-Trotter formula [15]–[19]. In particle physics, the massive Schwinger model has been studied using DMRG to confirm the well-known Coleman's picture of 'half-asymptotic' particles at a background field $\theta = \pi$ [20]. It is interesting to seek a possibility of applying the method to quantum chromodynamics (QCD) in order to study color confinement and spontaneous chiral symmetry breaking based on QCD vacuum wavefunctions.

In fermionic lattice models, the number of particles contained in each site is limited because of the Pauli principle. On the other hand, in bosonic lattice models, each site can contain infinite number of particles in principle. It is not evident whether Hilbert space can be described appropriately with a finite set of basis states in bosonic models. This point becomes crucial when DMRG is applied to gauge theories because gauge particles are bosons. Before working in lattice gauge theories like Kogut-Susskind hamiltonian [21], we need to test DMRG in a simple bosonic model and recognize how many basis states are necessary for each site to reproduce accurate results. In this paper, we apply DMRG to a $\lambda\phi^4$ model with (1+1) space-time dimensions. We define a hamiltonian model on a spatial lattice (only space is discretized) because DMRG is a method based on hamiltonian formalism. The model has spontaneous breakdown of discrete Z_2 symmetry and the exact values of the critical exponents are known. We are going to justify the relevance of DMRG truncation of Hilbert space in the bosonic model by comparing our numerical results with the Monte Carlo and the exact results [22, 23]. Our largest lattice size is $L = 1000$, which is about twice of the latest Monte Carlo one [22]. It is shown that the lattice size $L = 500$ is sufficiently close to the limit $L \to \infty$.

This paper is organized as follows. In section 2, hamiltonian lattice formulation of the model is given. The canonical variables are transformed to Fock-like operators, each of which creates or annihilates a boson on each site. Real-space representation is maintained because local interactions are useful for DMRG. In section 3, DMRG setup for the model is explained. A superblock is composed of two blocks and one site. Section 4 gives the definition of the critical values and shows numerical results. Section 5 is devoted to summary.

2. A $\lambda\phi^4_{1+1}$ hamiltonian lattice model

We start from the following lagrangian of a (1+1)-dimensional $\lambda\phi^4$ model

$$L_{\mathrm{c}} = \int dx \left[\frac{1}{2}(\partial_\mu \phi \partial^\mu \phi - \mu_0^2 \phi^2) - \frac{\lambda}{4!}\phi^4\right], \tag{2.1}$$

where space and time are continuous. Only the space is discretized to obtain a hamiltonian lattice model. In this paper, the spatial derivative is modeled as a naive difference on the lattice.[1] Lagrangian of the lattice model is

$$L = a\sum_{n=1}^{L}\left(\frac{1}{2}\dot{\phi}_n^2 - \frac{\mu_0^2}{2}\phi_n^2 - \frac{\lambda}{4!}\phi_n^4\right) - \frac{1}{2a}\sum_{n=1}^{L-1}(\phi_n - \phi_{n+1})^2\,, \tag{2.2}$$

[1] Discretization errors associated with the derivative can be improved in a systematic way by introducing non-nearest neighbor interactions [24, 25].

where a is a lattice spacing and time is continuous. Open boundary conditions are chosen. Hamiltonian is given by

$$H = \sum_{n=1}^{L} \left(\frac{1}{2a}\pi_n^2 + \frac{\mu_0^2 a}{2}\phi_n^2 + \frac{\lambda a}{4!}\phi_n^4 \right) + \frac{1}{2a}\sum_{n=1}^{L-1} \left(\phi_n - \phi_{n+1}\right)^2 , \tag{2.3}$$

where $\pi_n \equiv a\dot{\phi}_n$ is the conjugate variable to ϕ_n. All dimensionful quantities are measured in units of a.

$$\tilde{H} \equiv Ha\,, \qquad \tilde{\mu_0}^2 \equiv \mu_0^2 a^2\,, \qquad \tilde{\lambda} \equiv \lambda a^2\,. \tag{2.4}$$

To quantize the system, we impose an equal-time commutation relation

$$[\phi_m(t), \pi_n(t)] = i\delta_{mn}\,. \tag{2.5}$$

We rewrite hamiltonian (2.3) using creation and annihilation operators $a_n^\dagger$ and a_n.

$$\phi_n = \frac{1}{\sqrt{2}}\left(a_n^\dagger + a_n\right), \qquad \pi_n = \frac{i}{\sqrt{2}}\left(a_n^\dagger - a_n\right), \tag{2.6}$$

where $[a_m, a_n^\dagger] = \delta_{mn}$ and $a_n|0\rangle = 0$. Note that $a_n^\dagger$ and a_n are not creation and annihilation operators in Fock representation. The index n of the operators $a_n^\dagger$ and a_n stands for the discretized spatial coordinate, not momentum. Real-space representation is better for our purpose because local interactions are useful for DMRG. (See ref. [13, 14] for DMRG in momentum-space representation.)

In this model, figure 1 is the only diagram that diverges in the continuum limit $a \to 0$. The divergence can be renormalized by redefining the mass parameter as

$$\tilde{\mu}_0^2 = \tilde{\mu}^2 - \delta\tilde{\mu}^2\,,$$

where $\delta\tilde{\mu}^2$ is a counter term that cancels the divergence.

$$\delta\tilde{\mu}^2 = \frac{\lambda}{2}S_L(\tilde{\mu}^2)\,.$$

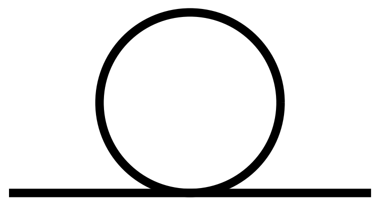

Figure 1: The only divergent diagram in the (1+1)-dimensional $\lambda\phi^4$ model.

S_L is given as a discrete sum because the system is quantized in a finite spatial box,

$$S_L(\tilde{\mu}^2) = \frac{1}{2L}\sum_{n=1}^{L} \frac{1}{\sqrt{\tilde{\mu}^2 + 4\sin^2\frac{\pi n}{L}}}\,. \tag{2.7}$$

In the limit $L \to \infty$, the sum (2.7) becomes

$$\begin{aligned} S_\infty(\tilde{\mu}^2) &= \frac{1}{2\pi}\int_0^1 dt \frac{1}{\sqrt{(t^2 + \frac{\tilde{\mu}^2}{4})(1-t^2)}} \\ &= \frac{1}{\pi\sqrt{\tilde{\mu}^2 + 4}} F\left(\frac{\pi}{2}, \frac{2}{\sqrt{\tilde{\mu}^2+4}}\right), \end{aligned} \tag{2.8}$$

where F is the elliptic integral of the first kind

$$F(\varphi, k) = \int_0^{\varphi} \frac{d\theta}{\sqrt{1 - k^2 \sin^2 \theta}} \, .$$

The integral S_∞ is used for all calculations of the counter term $\delta\tilde{\mu}^2$ even with a finite lattice because we are interested in the limit $L \to \infty$. We are going to calculate the critical coupling and exponent by extrapolating numerical data points to the limit $L \to \infty$.

In Fock representation, the divergence can be removed easily by taking normal ordering of hamiltonian. However, hamiltonian (2.3) cannot be normal-ordered easily because our representation is given in real space and different from Fock one. For this reason, we need to evaluate the integral (2.8) explicitly and redefine the mass parameter to renormalize the divergence in a numerical manner.

3. DMRG with one-site insertion

We are going to apply DMRG technique to the the model given in the previous section. In this paper, the system is composed of two renormalized blocks (system and environment blocks) and one bare site, each of which is approximated with a finite number of basis states. Based on the DMRG technique, basis states for system and environment blocks are optimized to describe the whole system in a finite dimensional space.

In fermionic models, dimension of hamiltonian is finite on a finite lattice. On the other hand, in bosonic models, each site can contain any number of bosons. Namely, each site has infinite degrees of freedom. The dimension of a bosonic hamiltonian is infinite even on a finite lattice. There is an essential difference between boson and fermion. To perform numerical calculations, hamiltonian needs to be finite dimensional because a computer can only take care of finite dimensional matrices. For this reason, in our bosonic model, the number of basis states of each bare site needs to be restricted when it is inserted between system and environment blocks. In the White's first paper for DMRG, two sites are inserted between system and environment blocks in each RG step [11, 12]. Since the model considered there is antiferromagnetic $S = 1/2$ Heisenberg chain, the total spin of the whole system needs to be kept constant for numerical stability. However, our model has no such a requirement associated with spins. When we insert bare sites between two blocks, a smaller number of sites is better. One-site insertion is the best choice.

We divide hamiltonian into two parts:

$$\tilde{H} = \sum_{n=1}^{L} h_n + \sum_{n=1}^{L-1} h_{n,n+1} \, , \tag{3.1}$$

where

$$\begin{aligned} h_n &= \frac{1}{2}\pi_n^2 + \frac{\tilde{\mu}_0^2}{2}\phi_n^2 + \frac{\tilde{\lambda}}{4!}\phi_n^4, \\ h_{n,n+1} &= \frac{1}{2}(\phi_n - \phi_{n+1})^2 \, . \end{aligned}$$

We are going to apply the finite system algorithm of DMRG to the hamiltonian. As shown in figure 2, a superblock hamiltonian $H_{\rm S}$ is composed of two blocks and one site:

$$H_{\rm S} = \bar{H}_{\rm L} + h_{n-1,n} + h_n + h_{n,n+1} + \bar{H}_{\rm R}\,, \tag{3.2}$$

where $\bar{H}_{\rm L}$ and $\bar{H}_{\rm R}$ are effective hamiltonian for the left and right blocks, respectively. $h_{n-1,n}$ ($h_{n,n+1}$) is an interaction between the left (right) block and the inserted n-th bare site. The superblock hamiltonian $H_{\rm S}$ is an effective hamiltonian for the original $\tilde{H}$.

Basis states for the superblock are

$$|i,j,k\rangle_n = |u_i^{(\rm L)}\rangle|j^{(n)}\rangle|v_k^{(\rm R)}\rangle\,, \tag{3.3}$$

where $\{|u_i^{(\rm L)}\rangle | i = 1,\ldots,M\}$ and $\{|v_k^{(\rm R)}\rangle | k = 1,\ldots,M\}$ are finite sets of basis states for the left and right blocks, respectively. $\{|j^{(n)}\rangle | j = 1,\ldots,N\}$ is a set of basis states for the n-th bare site inserted between the two blocks,

$$|j^{(n)}\rangle \equiv \frac{1}{\sqrt{(j-1)!}}(a_n^\dagger)^{j-1}|0\rangle\,, \qquad j = 1,\ldots,N\,. \tag{3.4}$$

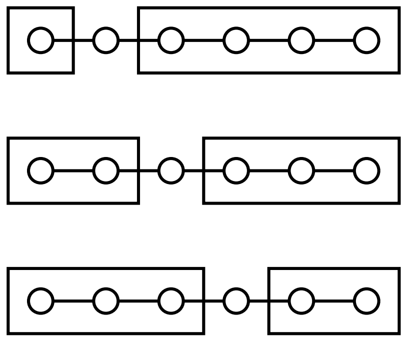

Figure 2: DMRG sweep process is shown. A superblock is composed of two renormalized blocks (system and environment) and one bare site. A bare site is moved from end to end. Basis states are optimized each time. One DMRG sweep is composed of L basis optimization steps.

At every DMRG step, basis states $\{|u_i^{(\rm L)}\rangle\}$ and $\{|v_k^{(\rm R)}\rangle\}$ are updated using the density matrix technique to renormalize the left and right block hamiltonian, $\bar{H}_{\rm L}$ and $\bar{H}_{\rm R}$. (See appendix A for the creation of basis states.) If M and N are infinite, the superblock hamiltonian $H_{\rm S}$ gives exact spectra because update of basis states is nothing but infinite dimensional unitary transformation. However, such a calculation is not possible on a finite computer. We truncate Hilbert space with finite M and N. The target state is expanded as

$$|\Psi\rangle = \sum_{i=1}^{M}\sum_{j=1}^{N}\sum_{k=1}^{M}\Psi_{ijk}|i,j,k\rangle_n\,. \tag{3.5}$$

The dimension of the superblock hamiltonian is M^2N. The relevance of truncation will be checked numerically by seeing convergence of energy and wavefunction with respect to the parameters M and N.

Matrix elements of the superblock hamiltonian are

$$\begin{aligned}{}_n\langle i,j,k|H_{\rm S}|i',j',k'\rangle_n = {} & \langle u_i^{(\rm L)}|\bar{H}_{\rm L}|u_{i'}^{(\rm L)}\rangle\delta_{jj'}\delta_{kk'} + \langle j^{(n)}|\langle u_i^{(\rm L)}|h_{n-1,n}|u_{i'}^{(\rm L)}\rangle|j'^{(n)}\rangle\delta_{kk'} + \\ & +\delta_{ii'}\langle j^{(n)}|h_n|j'^{(n)}\rangle\delta_{kk'} + \delta_{ii'}\langle j^{(n)}|\langle v_k^{(\rm R)}|h_{n,n+1}|v_{k'}^{(\rm R)}\rangle|j'^{(n)}\rangle + \\ & +\delta_{ii'}\delta_{jj'}\langle v_k^{(\rm R)}|\bar{H}_{\rm R}|v_{k'}^{(\rm R)}\rangle\,,\end{aligned} \tag{3.6}$$

where

$$\begin{aligned}\langle j^{(n)}|\langle u_i^{(\rm L)}|h_{n-1,n}|u_{i'}^{(\rm L)}\rangle|j'^{(n)}\rangle = {} & \frac{1}{2}\langle u_i^{(\rm L)}|\phi_{n-1}^2|u_{i'}^{(\rm L)}\rangle\delta_{jj'} - \langle u_i^{(\rm L)}|\phi_{n-1}|u_{i'}^{(\rm L)}\rangle\langle j^{(n)}|\phi_n|j'^{(n)}\rangle + \\ & +\frac{1}{2}\langle j^{(n)}|\phi_n^2|j'^{(n)}\rangle\delta_{ii'}\,,\end{aligned}$$

and

$$\langle j^{(n)}|\langle v_k^{(\mathrm{R})}|h_{n,n+1}|v_{k'}^{(\mathrm{R})}\rangle|j'^{(n)}\rangle = \frac{1}{2}\langle v_k^{(\mathrm{R})}|\phi_{n+1}^2|v_{k'}^{(\mathrm{R})}\rangle\delta_{jj'} - \langle v_k^{(\mathrm{R})}|\phi_{n+1}|v_{k'}^{(\mathrm{R})}\rangle\langle j^{(n)}|\phi_n|j'^{(n)}\rangle + \\ + \frac{1}{2}\langle j^{(n)}|\phi_n^2|j'^{(n)}\rangle\delta_{kk'}\,.$$

To calculate the matrix elements (3.6), the following matrix elements need to be calculated and stored at every DMRG step.

$$\begin{array}{ll} \langle u_i^{(\mathrm{L})}|\bar{H}_\mathrm{L}|u_{i'}^{(\mathrm{L})}\rangle\,, & \langle v_k^{(\mathrm{R})}|\bar{H}_\mathrm{R}|v_{k'}^{(\mathrm{R})}\rangle\,, \\ \langle u_i^{(\mathrm{L})}|\phi_{n-1}^2|u_{i'}^{(\mathrm{L})}\rangle\,, & \langle v_k^{(\mathrm{R})}|\phi_{n+1}^2|v_{k'}^{(\mathrm{R})}\rangle\,, \\ \langle u_i^{(\mathrm{L})}|\phi_{n-1}|u_{i'}^{(\mathrm{L})}\rangle\,, & \langle v_k^{(\mathrm{R})}|\phi_{n+1}|v_{k'}^{(\mathrm{R})}\rangle\,. \end{array}$$

Other matrix elements do not need to be stored because they can be calculated with operator contraction. (See appendix B.)

4. Numerical analysis

The critical values are defined with vacuum expectation values of the variable ϕ_n:

$$v(\tilde{\lambda},\tilde{\mu}^2) \equiv \langle\Psi_0|\phi_n|\Psi_0\rangle = A(\tilde{\lambda})\left[\frac{\tilde{\lambda}}{\tilde{\mu}^2} - \frac{\tilde{\lambda}}{\tilde{\mu}_\mathrm{c}^2(\tilde{\lambda})}\right]^{\beta(\tilde{\lambda})}, \tag{4.1}$$

where $|\Psi_0\rangle$ is a vacuum state and $A(\tilde{\lambda})$ is a constant dependent on $\tilde{\lambda}$. The vacuum expectation value v is calculated at the center $n = L/2$ using vacuum wavefunctions Ψ_{ijk} for each pair of $\tilde{\lambda}$ and $\tilde{\mu}^2$. The quantities $\tilde{\mu}_\mathrm{c}^2(\tilde{\lambda})$, $\beta(\tilde{\lambda})$, and $A(\tilde{\lambda})$ are determined by fitting v to obtained numerical data. The critical coupling $(\lambda/\mu^2)_\mathrm{c}$ and the critical exponent β are defined in the continuum limit $a \to 0$ as follows [22]:

$$\frac{\tilde{\lambda}}{\tilde{\mu}_\mathrm{c}^2(\tilde{\lambda})} = \left(\frac{\lambda}{\mu^2}\right)_\mathrm{c} + B\tilde{\lambda}\,, \tag{4.2}$$

$$\beta(\tilde{\lambda}) = \beta + C\tilde{\lambda}\,, \tag{4.3}$$

where B and C are some constants. In the continuum limit $a \to 0$, the coupling constant $\tilde{\lambda} = \lambda a^2$ vanishes. Then, we have

$$\left(\frac{\lambda}{\mu^2}\right)_\mathrm{c} = \lim_{\tilde{\lambda}\to 0}\frac{\tilde{\lambda}}{\tilde{\mu}_\mathrm{c}^2(\lambda)}\,, \qquad \beta = \lim_{\tilde{\lambda}\to 0}\beta(\tilde{\lambda})\,. \tag{4.4}$$

In numerical analysis, the continuum limit cannot be reached directly. The critical values $(\lambda/\mu^2)_\mathrm{c}$ and β are determined by extrapolating $\tilde{\lambda}/\tilde{\mu}_\mathrm{c}^2(\tilde{\lambda})$ and $\beta(\tilde{\lambda})$ to the continuum limit $\tilde{\lambda} = 0$. Also, finite-size effects on the critical values are removed by using sufficiently large lattices ($L = 250, 500$, and 1000).

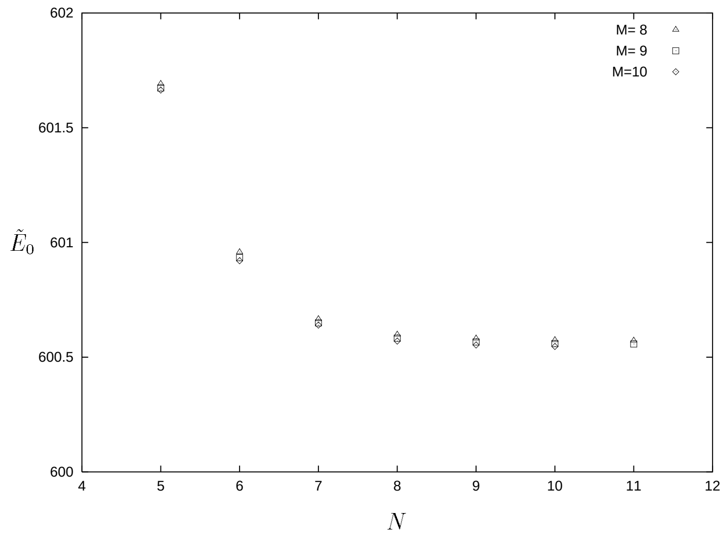

Figure 3: Vacuum energy $\tilde{E}_0 = E_0 a$ is plotted as a function of N for $M = 8, 9$, and 10. Coupling constant, bare mass squared, and lattice size are $\tilde{\lambda} = 0.6$, $\tilde{\mu}_0^2 = -0.2$, and $L = 1000$, respectively.

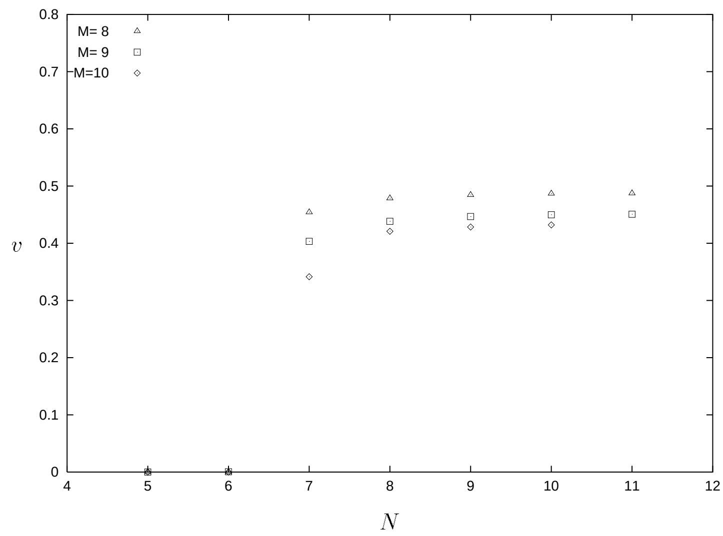

Figure 4: Vacuum expectation value v is plotted as a function of N for $M = 8, 9$, and 10. Coupling constant, bare mass squared, and lattice size are $\tilde{\lambda} = 0.6$, $\tilde{\mu}_0^2 = -0.2$, and $L = 1000$, respectively.

Figure 3 shows N dependence of vacuum energy $\tilde{E}_0 = E_0 a$ for each $M = 8, 9$, and 10. Values of the other parameters are $\tilde{\lambda} = 0.6$, $\tilde{\mu}_0^2 = -0.2$ ($\tilde{\mu}^2 = 9.744828 \times 10^{-3}$), and $L = 1000$. The energy converges as N increases with M fixed. Parameter values $(M, N) = (10, 10)$ gives convergence of vacuum energy in accuracy of four digits. Figure 4 shows N dependence of the vacuum expectation value v for each $M = 8, 9$, and 10. Other parameter values are same as figure 3. v converges at $N = 10$ for each M, but convergence for M with N fixed is slow. We will use the values $(M, N) = (10, 10)$ in all calculations to determine critical values.

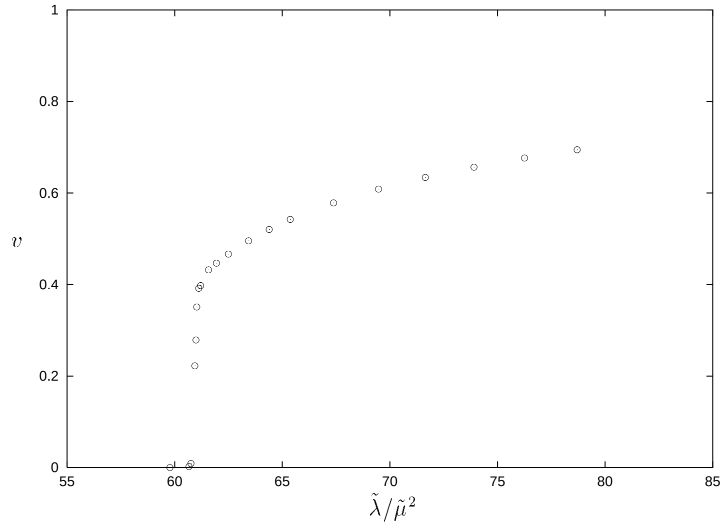

Figure 5: Vacuum expectation value v is plotted as a function of $\tilde\lambda/\tilde\mu^2$ with $\tilde\lambda = 0.6$ fixed. The lattice size is $L = 1000$.

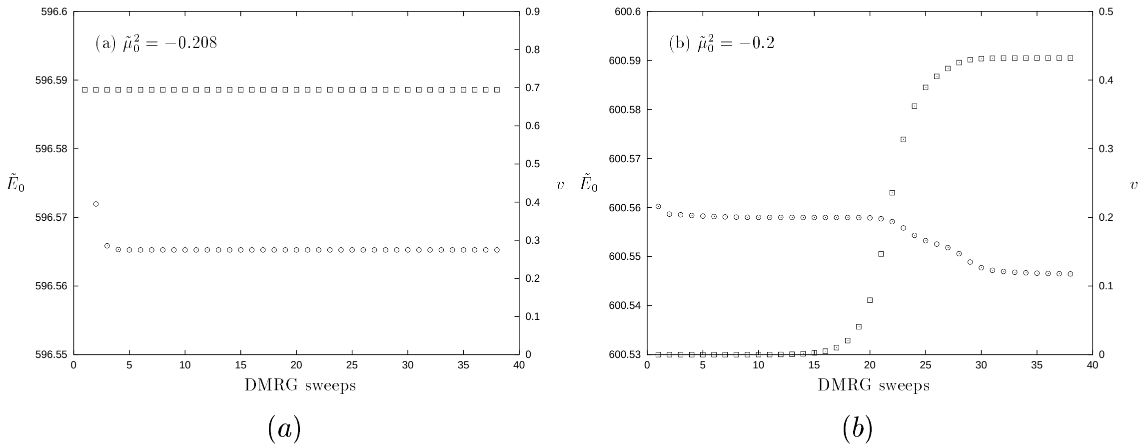

Figure 6: $\tilde E_0$ (circles) and v (squares) are plotted as functions of the number of DMRG sweeps for $\tilde\lambda = 0.6$, $L = 1000$, and $(M, N) = (10, 10)$. Convergence speed are compared between (a) $\tilde\mu_0^2 = -0.208$ ($\tilde\lambda/\tilde\mu^2 \sim 78.7$) and (b) $\tilde\mu_0^2 = -0.2$ ($\tilde\lambda/\tilde\mu^2 \sim 61.6$). Circles and squares represent $\tilde E_0$ and v, respectively. Data points are plotted every DMRG sweep.

In figure 5, vacuum expectation value $v(\tilde\lambda, \tilde\mu^2)$ is plotted as a function of $\tilde\lambda/\tilde\mu^2$ for a fixed $\tilde\lambda = 0.6$ on the lattice $L = 1000$. If $\tilde\lambda/\tilde\mu^2$ is decreased from the positive side, v becomes smaller and finally vanishes at a point $\tilde\lambda/\tilde\mu_c^2(\tilde\lambda)$. The obtained data points are fitted with eq. (4.1) to calculate $\tilde\mu_c^2(\tilde\lambda)$ and $\beta(\tilde\lambda)$ for each $\tilde\lambda$. The Marquardt-Levenberg nonlinear least-squares algorithm is used for fitting. Similar figures are drawn also for $\tilde\lambda = 1.5$ and 3.0 to determine $\tilde\mu_c^2(\tilde\lambda)$ and $\beta(\tilde\lambda)$.

In figure 6, $\tilde E_0$ and v are plotted as functions of the number of DMRG sweeps for $\tilde\lambda = 0.6$ and $L = 1000$. Convergence speed is compared between $\tilde\mu_0^2 = -0.208$ ($\tilde\lambda/\tilde\mu^2 \sim 78.7$) and $\tilde\mu_0^2 = -0.2$ ($\tilde\lambda/\tilde\mu^2 \sim 61.6$). The former and latter parameter values correspond to the first

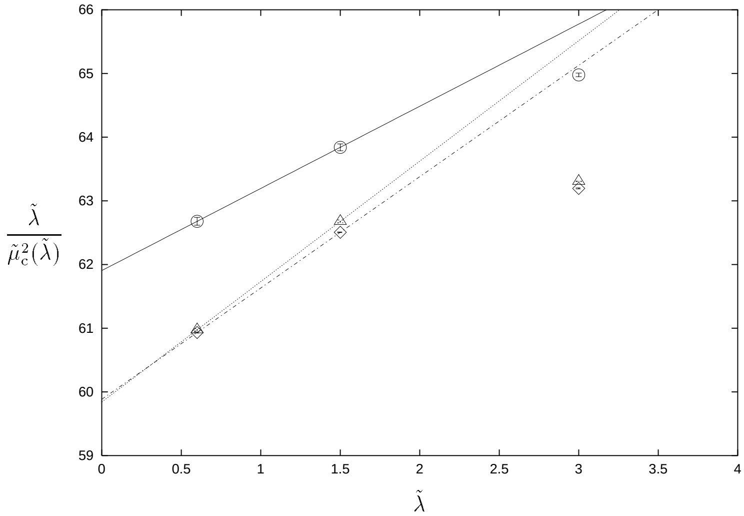

Figure 7: The ratio $\tilde{\lambda}/\tilde{\mu}_{\mathrm{c}}^2(\tilde{\lambda})$ is plotted as a function of the coupling constant $\tilde{\lambda}$ $(= 0.6, 1.5, 3.0)$ for three lattice sizes $L = 250$ (circles), 500 (triangles), and 1000 (diamonds). Each plot is fitted with a straight line to determine $(\lambda/\mu^2)_{\mathrm{c}}$ in the limit $\tilde{\lambda} \to 0$. The fitted lines are drawn with solid $(L = 250)$, dotted $(L = 500)$, and dot-dashed $(L = 1000)$ lines.

and twelfth points from the right hand side in figure 5, respectively. The latter is close to the critical value $\tilde{\lambda}/\tilde{\mu}_{\mathrm{c}}^2(\tilde{\lambda})|_{\tilde{\lambda}=0.6}$. In figure 6, data points are plotted every DMRG sweep. One DMRG sweep is composed of $L = 1000$ sets of basis state optimization. Convergence tends to be slow as $\tilde{\lambda}/\tilde{\mu}^2$ approaches the critical value. When $\tilde{\mu}_0^2 = -0.208$, convergence of both quantities is very fast. On the other hand, when $\tilde{\mu}_0^2 = -0.2$, energy converges in accuracy of four digits even with a small number of DMRG sweeps, but convergence of v is slow. v barely converges in the latter case. Because of limited computer time, complete convergence is not available for v when $\tilde{\mu}^2$ is very close to the critical value $\tilde{\mu}_{\mathrm{c}}^2(\tilde{\lambda})$. We calculate $\tilde{E}_0$ and v with up to forty DMRG sweeps checking their convergence to determine $\tilde{\mu}_{\mathrm{c}}^2(\tilde{\lambda})$ on each lattice.

In figure 7, the ratio $\tilde{\lambda}/\tilde{\mu}_{\mathrm{c}}^2(\tilde{\lambda})$ is plotted as a function of $\tilde{\lambda}$ $(= 0.6, 1.5, 3.0)$ with error bars for three lattice sizes $L = 250$, 500, and 1000. The errors come from fitting. We are going to take the continuum limit $a \to 0$ to determine the values of $(\lambda/\mu^2)_{\mathrm{c}}$. As explained in eq. (4.2), the data points are fitted with a straight line and extrapolated to the limit $\tilde{\lambda} \to 0$ for each L. The data points for $\tilde{\lambda} = 0.6$ and 1.5 are used for fitting and extrapolation.

Figure 8 plots the extrapolated values $(\lambda/\mu^2)_{\mathrm{c}}$ as a function of $1/L$. We observe good agreement between the two results for $L = 500$ and 1000. That is, the lattice size $L = 500$ is sufficiently large and close to the limit $L \to \infty$. For this reason, we fit the two points for $L = 500$ and 1000 with a straight line to extrapolate them to the limit $L \to \infty$. In the continuum limit $a \to 0$ and $L \to \infty$, we obtain $(\lambda/\mu^2)_{\mathrm{c}} = 59.89 \pm 0.01$. Our result is close to the euclidean Monte Carlo result [22], which has been given with lattices up to $L = 512$. No exact result for $(\lambda/\mu^2)_{\mathrm{c}}$ has been known. Table 1 shows various results for the critical value $(\lambda/\mu^2)_{\mathrm{c}}$.

JHEP05(2004)007

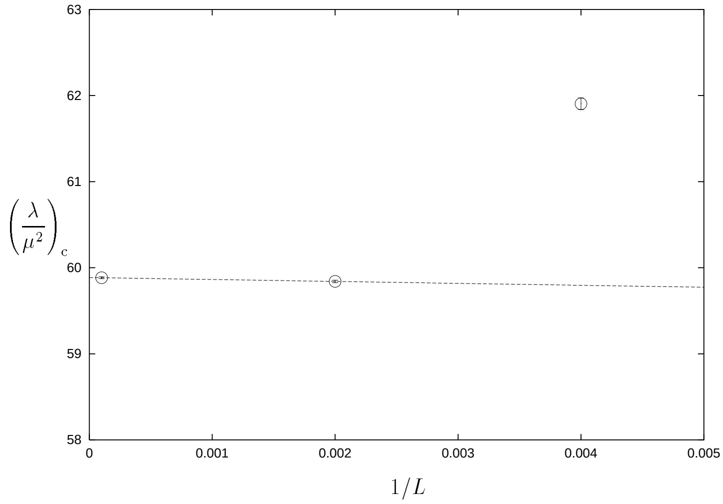

Figure 8: The critical value $(\lambda/\mu^2)_c$ is plotted as a function of $1/L$ for $L = 250, 500$, and 1000. Extrapolation to the limit $L \to \infty$ gives $(\lambda/\mu^2)_c = 59.89 \pm 0.01$.

Method	Result	Reference
DMRG	59.89 ± 0.01	this work
Monte Carlo	$61.56^{+0.48}_{-0.24}$	[22]
Gaussian effective potential	61.266	[26]
Gaussian effective potential	61.632	[31]
Connected Green function	58.704	[31]
Coupled cluster expansion	$22.8 < (\lambda/\mu^2)_c < 51.6$	[27]
Non-gaussian variational	41.28	[30]
Discretized light cone	43.896, 33.000	[28, 29]
Discretized light cone	42.948, 46.26	[5]

Table 1: Various results for the critical coupling constant $(\lambda/\mu^2)_c$ are listed. Our result is consistent with the Monte Carlo result.

Figure 9 plots the critical exponent $\beta(\tilde{\lambda})$ as a function of $\tilde{\lambda}$ $(= 0.6, 1.5, 3.0)$ for $L = 250$, 500, and 1000. As before, the data points are fitted with eq. (4.3) and extrapolated to the limit $\tilde{\lambda} = 0$ for each L. The data points for $\tilde{\lambda} = 0.6$ and 1.5 are used for fitting and extrapolation. Figure 10 plots the extrapolated values $\beta(0)$ as a function of $1/L$. Also in this case, we observe that the results for $L = 500$ and 1000 are very close. Extrapolation with these two points to the limit $L \to \infty$ gives the critical exponent $\beta = 0.1264 \pm 0.0073$. No Monte Carlo result for the critical exponent β is available in the literature at this point. According to the universality class consideration, the critical exponents of the (1+1)-dimensional $\lambda\phi^4$ model are same as the two-dimensional Ising model, which has been exactly solved by Onsager [23]. Our result is consistent with the exact value $\beta = 1/8 = 0.125$. As seen from figure 8 and 10, the lattice size $L = 500$ is sufficiently close to the limit $L \to \infty$.

JHEP05(2004)007

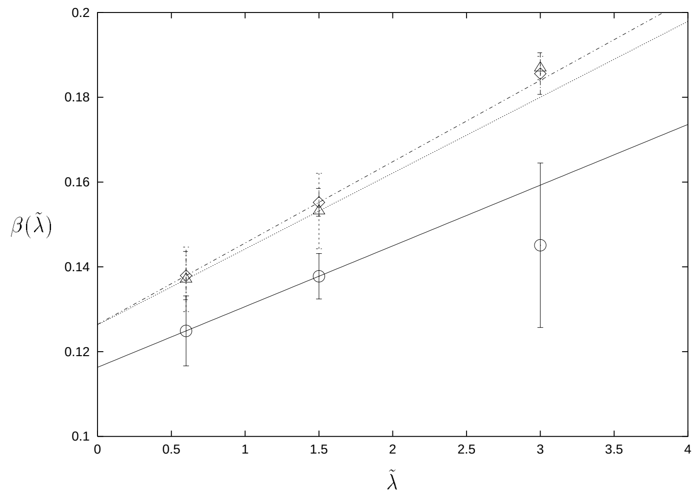

Figure 9: $\beta(\tilde{\lambda})$ is plotted as a function of the coupling constant $\tilde{\lambda}$ $(= 0.6, 1.5, 3.0)$ for three lattice sizes $L = 250$ (circles), 500 (triangles), and 1000 (diamonds). Each plot is fitted with a straight line to determine $\beta(0)$. Fitted lines are drawn with solid (L=250), dotted ($L = 500$), and dot-dashed ($L = 1000$) lines.

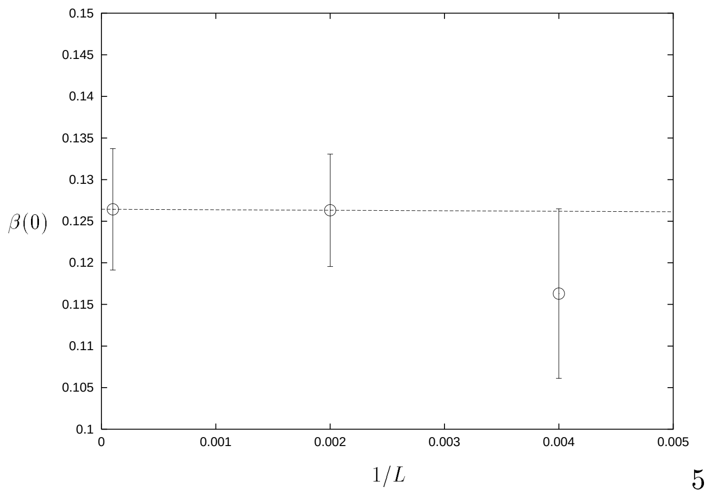

Figure 10: $\beta(0)$ is plotted as a function of $1/L$ for $L = 250, 500,$ and 1000. Extrapolation to the limit $L \to \infty$ gives $\beta = 0.1264 \pm 0.0073$, which is consistent with the exact result $\beta = 1/8 = 0.125$.

5. Summary

We have studied spontaneous breakdown of Z_2 symmetry of a (1+1)-dimensional ϕ^4 model using the density matrix renormalization group technique. We have determined the critical coupling constant $(\lambda/\mu^2)_{\rm c}$ and the critical exponent β of the model by extrapolating the numerical results for finite lattices to the continuum limit $a \to 0$ and $L \to \infty$. DMRG truncation works well also in the bosonic model. The lattice with $L = 500$ can give results sufficiently close to the limit $L \to \infty$. To improve calculations near $\tilde{\mu}_{\rm c}^2(\tilde{\lambda})$, we need to find a way to include effects of large quantum fluctuations.

JHEP05(2004)007

Acknowledgments

The numerical calculations were carried on RIKEN VPP and Yukawa Institute SX5. This work has been partially supported by RIKEN.

A. Basis states and density matrices

This is a brief explanation of basis state creation with the density matrix technique, which is the key ingredient of DMRG. We split a spatial lattice into left and right blocks, each of which are expressed with basis sets $\{|i^{(\mathrm{L})}\rangle | i=1,2,\ldots,N_{\mathrm{L}}\}$ and $\{|j^{(\mathrm{R})}\rangle | j=1,2,\ldots,N_{\mathrm{R}}\}$, respectively. The target state to be solved is expanded as

$$|\Psi\rangle = \sum_{i=1}^{N_{\mathrm{L}}}\sum_{j=1}^{N_{\mathrm{R}}} \Psi_{ij}|i^{(\mathrm{L})}\rangle|j^{(\mathrm{R})}\rangle\,, \qquad N_{\mathrm{L}} \le N_{\mathrm{R}}\,. \tag{A.1}$$

When N_{L} and N_{R} are sufficiently small, we can obtain wavefunction of a target state (say ground state) by diagonalizing hamiltonian numerically. If the basis states $\{|i^{(\mathrm{L})}\rangle\}$ and $\{|j^{(\mathrm{R})}\rangle\}$ are transformed, the wavefunction Ψ_{ij} is also transformed. We want to make the absolute values of the wavefunction components very small as many as possible, because basis states giving very small wavefunction component are not important for the target state $|\Psi\rangle$ and can be thrown away. We transform basis states based on the following singular-value decomposition.

$$\Psi_{ij} = \sum_{k=1}^{N_{\mathrm{L}}} U_{ik} D_k V_{kj}\,, \tag{A.2}$$

where

$$\sum_{i=1}^{N_{\mathrm{L}}} U^*_{ik} U_{ik'} = \delta_{kk'}\,, \qquad \sum_{j=1}^{N_{\mathrm{R}}} V^*_{kj} V_{k'j} = \delta_{kk'}\,.$$

In the new basis

$$|u_k^{(\mathrm{L})}\rangle = \sum_{i=1}^{N_{\mathrm{L}}} U_{ik}|i^{(\mathrm{L})}\rangle\,, \qquad |v_k^{(\mathrm{R})}\rangle = \sum_{j=1}^{N_{\mathrm{R}}} V_{kj}|j^{(\mathrm{R})}\rangle\,,$$

the target state becomes

$$|\Psi\rangle = \sum_{k=1}^{N_{\mathrm{L}}} D_k |u_k^{(\mathrm{L})}\rangle|v_k^{(\mathrm{R})}\rangle\,. \tag{A.3}$$

The result does not change largely even if a basis state with small D_k is removed from the calculation. On the other hand, a basis state with large D_k is important and cannot be neglected. We can use D_k's to choose good basis states and control calculation accuracy. In actual numerical works, we diagonalize the following density matrices to obtain U, V, and D in stead of performing singular-value decomposition directly.

$$\rho^{(\mathrm{L})}_{ii'} = \sum_{j=1}^{N_{\mathrm{R}}} \Psi^*_{ij}\Psi_{i'j} = \sum_{k=1}^{N_{\mathrm{L}}} U^*_{ik}|D_k|^2 U_{i'k}\,,$$

$$\rho^{(\mathrm{R})}_{jj'} = \sum_{i=1}^{N_{\mathrm{L}}} \Psi^*_{ij}\Psi_{ij'} = \sum_{k=1}^{N_{\mathrm{L}}} V^*_{kj}|D_k|^2 V_{kj'}\,.$$

See ref. [19] for the details of DMRG and related topics.

B. Matrix elements

This appendix gives formulas for matrix elements of powers of the field operators π_n and ϕ_n. For the definition of the basis states $|j^{(n)}\rangle$, see eq. (3.4).

$$\begin{aligned}
\langle j^{(n)}|\pi_n^2|j'^{(n)}\rangle &= \frac{1}{2}\Big[-\sqrt{(j-1)(j-2)}\,\delta_{j-1,j'+1} + (2j-1)\delta_{j,j'} - \sqrt{(j'-1)(j'-2)}\,\delta_{j+1,j'-1}\Big]\,,\\
\langle j^{(n)}|\phi_n|j'^{(n)}\rangle &= \frac{1}{\sqrt{2}}\Big[\sqrt{j-1}\,\delta_{j-1,j'} + \sqrt{j'-1}\,\delta_{j,j'-1}\Big]\,,\\
\langle j^{(n)}|\phi_n^2|j'^{(n)}\rangle &= \frac{1}{2}\Big[\sqrt{(j-1)(j-2)}\,\delta_{j-1,j'+1} + (2j-1)\delta_{j,j'} + \sqrt{(j'-1)(j'-2)}\,\delta_{j+1,j'-1}\Big]\,,\\
\langle j^{(n)}|\phi_n^4|j'^{(n)}\rangle &= \frac{1}{4}\Big[\sqrt{(j-1)(j-2)(j-3)(j-4)}\,\delta_{j-1,j'+3} + 4j\sqrt{(j-1)(j-2)}\,\delta_{j,j'+2} -\\
&\quad - 6\sqrt{(j-1)(j-2)}\,\delta_{j-1,j'+1} + 3(2j^2-2j+1)\delta_{j,j'} +\\
&\quad + 4j'\sqrt{(j'-1)(j'-2)}\,\delta_{j+2,j'} - 6\sqrt{(j'-1)(j'-2)}\,\delta_{j+1,j'-1} +\\
&\quad + \sqrt{(j'-1)(j'-2)(j'-3)(j'-4)}\,\delta_{j+3,j'-1}\Big]\,.
\end{aligned}$$

References

[1] H. Bethe, *On the theory of metals, 1. Eigenvalues and eigenfunctions for the linear atomic chain*, *Z. Phys.* **71** (1931) 205–226.

[2] C.-N. Yang, *Some exact results for the many body problems in one dimension with repulsive delta function interaction*, *Phys. Rev. Lett.* **19** (1967) 1312.

[3] K. Harada, T. Sugihara, M.-a. Taniguchi and M. Yahiro, *The massive schwinger model with* $\mathrm{SU}(2)_f$ *on the light cone*, *Phys. Rev.* **D 49** (1994) 4226 [hep-th/9309128].

[4] T. Sugihara, M. Matsuzaki and M. Yahiro, *Two-dimensional* $\mathrm{SU}(N)$ *gauge theory on the light cone*, *Phys. Rev.* **D 50** (1994) 5274 [hep-th/9402092].

[5] T. Sugihara, *Variational calculation of the effective action*, *Phys. Rev.* **D 57** (1998) 7373 [hep-th/9711129].

[6] T. Sugihara and M.-A. Taniguchi, *Manifestation of a nontrivial vacuum in discrete light-cone quantization*, *Phys. Rev. Lett.* **87** (2001) 271601 [hep-th/0104012].

[7] T. Sugihara, *Basis optimization renormalization group for quantum hamiltonian*, *Nucl. Phys.* **108** *(Proc. Suppl.)* (2002) 267 [hep-th/0104013].

[8] N. Sakai and M. Sakamoto, *Lattice supersymmetry and the Nicolai mapping*, *Nucl. Phys.* **B 229** (1983) 173.

[9] P. Fendley, K. Schoutens and J. de Boer, *Lattice models with* $N = 2$ *supersymmetry*, *Phys. Rev. Lett.* **90** (2003) 120402 [hep-th/0210161].

[10] K.G. Wilson, *The renormalization group: critical phenomena and the kondo problem*, *Rev. Mod. Phys.* **47** (1975) 773.

[11] S.R. White, *Density matrix formulation for quantum renormalization groups*, *Phys. Rev. Lett.* **69** (1992) 2863.

[12] S.R. White, *Density-matrix algorithms for quantum renormalization groups*, *Phys. Rev.* **B 48** (1993) 10345.

[13] T. Xiang, *Density-matrix renormalization-group method in momentum space*, *Phys. Rev.* **B 53** (1996) R10445.

[14] T. Xiang, J. Lou and Z. Su, *Two-dimensional algorithm of the density-matrix renormalization group*, *Phys. Rev.* **B 64** (2001) 104414.

[15] R.J. Bursill, T. Xiang and G.A. Gehring, *The density matrix renormalization group for a quantum spin chain at non-zero temperature*, *J. Phys.: Condens. Matter* **8** (1996) L583.

[16] X. Wang and T. Xiang, *Transfer-matrix density-matrix renormalization-group theory for thermodynamics of one-dimensional quantum systems*, *Phys. Rev.* **B 56** (1997) 5061.

[17] T. Xiang, *Thermodynamics of quantum Heisenberg spin chains*, *Phys. Rev.* **B 58** (1998) 9142.

[18] N. Shibata, *Thermodynamics of the anisotropic Heisenberg chain calculated by the density matrix renormalization group method*, *J. Phys. Soc. Jpn.* **66** (1997) 2221.

[19] I. Peschel, X. Wang, M. Kaulke and K. Hallberg (Eds.), *Density-matrix renormalization: a new numerical method in physics*, Springer-Verlag, Berlin 1999.

[20] T. Byrnes, P. Sriganesh, R.J. Bursill and C.J. Hamer, *Density matrix renormalisation group approach to the massive schwinger model*, *Phys. Rev.* **D 66** (2002) 013002 [hep-lat/0202014].

[21] J.B. Kogut and L. Susskind, *Hamiltonian formulation of Wilson's lattice gauge theories*, *Phys. Rev.* **D 11** (1975) 395.

[22] W. Loinaz and R.S. Willey, *Monte Carlo simulation calculation of critical coupling constant for two-dimensional continuum ϕ^4*, *Phys. Rev.* **D 58** (1998) 076003 [hep-lat/9712008].

[23] L. Onsager, *Crystal statistics. I. a two-dimensional model with an order-disorder transition*, *Phys. Rev.* **65** (1944) 117.

[24] T. Sugihara, *Lattice chiral symmetry with nonlocal interactions*, *Phys. Rev.* **D 68** (2003) 034502 [hep-lat/0304015].

[25] T. Sugihara, *Vector and chiral gauge theories on the lattice*, hep-lat/0310061.

[26] S.-J. Chang, *The existence of a second order phase transition in the two-dimensional ϕ^4 field theory*, *Phys. Rev.* **D 13** (1976) 2778, erratum *ibid.* **D16** (1976) 1979.

[27] M. Funke, U. Kaulfuss and H. Kummel, *Approaching the critical region of two-dimensional ϕ^4 quantum field theory with postgaussian approximations*, *Phys. Rev.* **D 35** (1987) 621.

[28] A. Harindranath and J.P. Vary, *Solving two-dimensional ϕ^4 theory by discretized light front quantization*, *Phys. Rev.* **D 36** (1987) 1141.

[29] A. Harindranath and J.P. Vary, *Stability of the vacuum in scalar field models in* $1+1$ *dimensions*, *Phys. Rev.* **D 37** (1988) 1076.

[30] L. Polley and U. Ritschel, *Second order phase transition in lambda ϕ^4 in two-dimensions with nongaussian variational approximation*, *Phys. Lett.* **B 221** (1989) 44.

[31] J.M. Hauser, W. Cassing, A. Peter and M.H. Thoma, *Connected green function approach to ground state symmetry breaking in ϕ^4 in $(1+1)$-dimensions theory*, *Z. Phys.* **A353** (1996) 301 [hep-ph/9408355].